Final Report

Improved Forecasting of Extreme Rainfall Events Associated with Tropical Cyclones

NOAA Award NA13NWS4680005

FSU Account 520-032503

Henry Fuelberg
hfuelberg@fsu.edu

Robert Hart
rhart@fsu.edu

Tristan Hall
tjh10c@my.fsu.edu

Florida State University

29 November 2017

Table of Contents

1. Research goals and objectives

Much remains to be learned about the physical processes that affect rainfall patterns and amounts associated with landfalling tropical cyclones (TCs). This need is evident by the frequent major discrepancies between the forecast and observed patterns and amounts of rainfall.

This research uses existing knowledge about the physical processes in TCs that determine rainfall patterns and amounts to create a statistical forecast product. The final guidance product, which considers processes/parameters that are both internal and external to the TC, will be in a map format that shows the expected rainfall. The parameters selected for the statistical guidance will improve our understanding of model-derived rainfall estimates. We will use the results of the derived forecast product and GFS forecasts to determine the important environmental parameters that are needed to accurately predict TC rainfall.

In addition to our statistically-derived rainfall product, we will gain a qualitative understanding of meteorological conditions which lead to a skillful GFS TC rainfall forecast. GFS TC rainfall forecasts are separated into three categories, “Top, Middle, and Bottom”, and each is investigated to determine what meteorological conditions occur when the GFS is performing well (Top) or poorly (Bottom) with respect to TC rainfall. This will enable forecasters to identify key meteorological conditions that are regularly seen in good or bad GFS rainfall forecasts to determine if they can have confidence in GFS TC rainfall performance.

The specific objectives outlined in the original CSTAR proposal were:

1. Develop a real-time rainfall forecast product (through 5 days lead time) that can be track adjusted within the NHC forecast cone to provide important contingency forecasts for NWS offices and River Forecast Centers.
2. Provide an objective analysis of model bias to provide forecasters with a better understanding of when to trust the model guidance, and for model developers to further focus their improvement efforts.
3. Identify important environmental parameters that could lead to better TC precipitation forecasts in the future.
4. Improve rainfall distribution forecasts to uphold the NWS mission and to prevent public outcry during over and under forecasted events

We have updated some of the original objectives to better-align with what we were discovering during the preliminary stages of the research. The updated objectives are:

1. Develop a real-time rainfall forecast guidance product (through 3 days lead time) based on storm shear, intensity, motion, and regional characteristics.
2. Identify important meteorological conditions to provide guidance on guidance of GFS TC rainfall forecast skill.
3. Improve our understanding of TC rainfall forecasts and thereby improve the forecasts themselves to further uphold the NWS mission.

2. Motivation

2. 1. Brief literature review of hurricane rainfall structure

During the grant period, Tristan Hall wrote and defended his doctoral prospectus which had the same research objectives as the grant proposal (outlined above). Excerpts from the prospectus document follow. Topics that pertain to the methodologies behind the development of our statistical model as well as GFS rainfall skill are stressed.

2. 1. 1. TC rainfall structure and maintenance

The creation and evolution of rainfall within a TC is a complicated process. There are four common physical processes associated with rainfall in TCs: 1) water vapor flux convergence in the lower troposphere, 2) upward vertical motion, 3) potential instability, and 4) boundary layer convergence (Elsberry 1995). Ascending motion is found over large areas where torrential rains occur, and since TCs are primarily convective in nature, potential instability plays a key role in the initiation and sustainability of convection. The four processes are interconnected: boundary layer convergence leads to upward vertical motion, and low-level moisture transport is necessary to maintain potential instability. No research, to our knowledge, has been done to conclude whether any of these factors, or any other meteorological conditions, contribute to accurate GFS TC rainfall forecasts. This work seeks to remedy that.

2. 1. 2. The effect of vertical wind shear, TC translational speed, and storm intensity

TC motion and structure, and therefore rainfall, are modulated by vertical shear (e.g., Shapiro 1983; Jones 1995; Bender 1997; Frank and Ritchie 1999 2001; Reasor et al. 2013). These papers found that a moderate vertical tilt in the TC vortex due to vertical shear creates a

thermal wind imbalance. To correct this imbalance, a secondary circulation develops in both barotropic and baroclinic models (Jones 1995; Frank and Ritchie 1999, 2001). Jones (1995) and Frank and Ritchie (2001) found that the primary initiation location of convection was downshear-right (DSR). The evolution of convection was further explained and emphasized by Black et al. (2002; their Fig. 17). Their study supports the finding of convective initiation in the DSR quadrant. They also described the lifespan of convection: After the convection was initiated, the rotating, tangential winds of the TC advected the precipitation around the storm. Warm rainfall processes occurred during this time, and rain began to fall in the downshear-left (DSL) quadrant. When the original updraft that was associated with the convection reached the upshear side, it was above the 0° C level, and the low-levels were dominated by downdrafts. The remaining frozen condensate subsequently fell out; the updrafts accelerated upward and detached from the eyewall, and finally exited the storm in the upshear-right quadrant.

Vertical wind shear is the dominant factor that organizes precipitation and convection within a TC (Corbosiero and Molinari 2003; Wingo and Cecil 2010; Hence and Houze 2011; Reasor et al. 2013; Xu et al. 2014). Observationally, based on satellite (Chen et al. 2006; Wingo and Cecil 2010; Xu et al. 2014) and radar (Marks et al. 1992; Reasor et al. 2013) data, greatest precipitation asymmetries have been found in the DSL quadrant. The amplitude of the asymmetry increased with increasing strength of the shear (Rogers et al. 2003; Chen et al. 2006; Wingo and Cecil 2010; Xu et al. 2014). However, when shear was minimal, Chen et al. (2006) found that the effect of storm motion is comparable to the effect of shear in explaining TC precipitation asymmetries.

A wavenumber-1 asymmetry in precipitation was found by Lonfat et al. (2004), with maximum precipitation located in the front quadrants with respect to storm motion. The maximum asymmetry shifted from the forward left to the forward right quadrant as storm intensity increased. Furthermore, as the translational speed of the storm increased, the front-to-back asymmetry also increased. These asymmetries in precipitation are caused by increased asymmetrical frictional forcing due to increased storm motion and tangential wind speed (Shapiro 1983). The asymmetrical frictional forcing also can be seen with increasing storm motion (Frank and Ritchie 1999).

The modulation of rainfall due to vertical wind shear plays a key role in the creation of our statistical rainfall model. It is the primary factor which creates our statistical rainfall forecasts (described later). The motion-relative relationship is secondary. This hierarchy is based on Chen et al. (2006). Results from these previously mentioned theoretical and observational papers are compared to our regional Stage IV rainfall datasets in later sections of this report.

2. 1. 3. Other factors modulating TC rainfall

Although vertical wind shear is the dominant factor organizing precipitation and convection within a TC, additional environmental factors exterior and independent of the storm must be considered. Topographic effects influence a TC's precipitation distribution and amount (Haggard et al. 1973; Simpson and Riehl 1981; Rogers et al. 2009; Lonfat et al. 2007). Therefore, we divide the U.S. into seven different geographical regions to highlight unique regional characteristics, either due to topography or latitudinal differences (e.g., more barotropic or baroclinic in nature), that otherwise would be over-simplified in a full U.S. composite (described further in the Methodology Section).

The accumulation of rainfall also depends on storm track. For example, vertical shear can realign the precipitation, but the orientation of the shear and motion vectors can create different precipitation patterns (Rogers et al. 2003, their Fig. 21; Lonfat et al. 2007).

2. 1. 4. Satellite v. Stage IV data

2. 1. 4. 1 Stage IV rainfall data

The NCEP Stage IV dataset (Lin and Mitchell 2005) is a national mosaic of radar-, and gauge-based precipitation measurements on a 4 × 4 km grid. It is the primary rainfall data source for the creation of our statistical rainfall model and is used as observations in the investigation into GFS TC rainfall skill.

The twelve River Forecast Centers (RFCs) use their own rainfall algorithm to produce the rainfall estimates that comprise Stage IV. After the rainfall algorithms produce a product, each RFC then applies its own manual quality control (QC) to their respective regions input to the Stage IV dataset. In addition to differences in the RFC algorithms and QC procedures, inappropriate Z-R relationships can affect rainfall estimation at each radar site (Fulton et al. 1998). Similarly, there also are radar-specific uncertainties and errors that can adversely impact

precipitation estimates, such as poor radar calibration, attenuation, ground clutter, and beam blockage. It has been found that the correlation between Z and R is better closer to the radar (Villarini and Krajewski 2010). Since there are no gauges over water, only the Stage IV data within 150 km of the nearest coastal radar were used. Finally, hurricane-strength winds can affect the ability of a rain gauge to collect data. The accuracy of a gauge decreases with increasing wind speed (e.g., Miller 1958; Simpson and Riehl 1981).

The Stage IV dataset has been used in numerous TC studies. For example, Stage IV has been employed to validate TrAP techniques (Ferraro et al. 2005; Lonfat et al. 2007; Habib et al. 2009; Ebert et al. 2011; Zagrodnik and Jiang 2013), to evaluate model or satellite performance of TC precipitation (Marchok et al. 2007; Villarini et al. 2011), and to highlight inter-storm differences (Jiang et al. 2008). Despite the limitations of the Stage IV dataset, it still is the superior option compared to other CONUS precipitation datasets (the TRMM Multiple Satellite Precipitation Analysis [TMPA] and the North American Land Data Assimilation System [NLDAS]) for landfalling TCs (Villarini et al. 2011).

2. 1. 4. 2 Comparison between Stage IV and satellite data

The previously described papers show that TC rainfall structure is a complicated, dynamic process that has been studied extensively. However, those studies primarily focused on observations from radar or satellites. These platforms provide instantaneous rain rates, and one needs to extrapolate them to acquire the accumulation of rainfall during a period. Additionally, while these studies provide a useful climatology, the TCs that were aggregated were primarily over water (e.g., Lonfat et al. 2004). However, rainfall patterns and amounts over land can be different from those over water due to the interaction with the land surface (Simpson and Riehl 1981). Furthermore, the satellites used for these studies have latitudinal limits, which can cause a misrepresentation of TC rainfall for high-latitude storms. This is problematic for high-latitude storms that are beyond the satellite's scope, but still well-within the U.S. coastline. Therefore, Stage IV data (a combination of radar- and guage-derived amounts) are expected to provide a more-accurate representation of TC rainfall at landfall, especially when aggregating the data on a regional basis. Additionally, Scofield and Kuligowski (2003) and Villarini et al. (2011) found that Stage IV data were superior to their satellite-derived counterpart. Our rainfall dataset is

derived from Stage IV, and is the "ground truth" that we use for comparison with GFS-derived rainfall forecasts.

2. 2. Brief literature review of existing TC rainfall guidance tools

One of the goals of this research was to build on accumulated knowledge to better-forecast TC rainfall. This section briefly reviews previous TC rainfall guidance models.

2. 2. 1. R-CLIPER

The Rainfall Climatology and Persistence Model (R-CLIPER; Marks et al. 2002) provides a baseline persistence forecast based on satellite observations from Lonfat et al. (2004). The approach models TC rainfall via a parametric equation. The pattern of rainfall is linear from the storm center to the radius of climatological maximum rainfall, and then exponentially decays out to 500 km. It is dependent on the climatological radius of maximum rainfall and the mean rainfall rate. These values are dependent on storm intensity.

While R-CLIPER is an excellent base-line climatological persistence forecast, its rainfall signature can only change in magnitude due to storm intensity and/or motion (including speed and directional changes). The symmetric nature of R-CLIPER does not account for shear or regional characteristics which can make TC rainfall asymmetric. Marks et al. (2002) indicated that “more than a simple rain model with a peak along the track is needed (e.g., one with asymmetries)." Our statistical rainfall product improves on R-CLIPER by using an aggregated observational dataset instead of a parameterized model. It also incorporates shear, motion, and intensity, and the regional differences between them.

2. 2. 2. PHRaM

The Parametric Hurricane Rainfall Model (PHRaM; Lonfat et al. 2007) attempts to update R-CLIPER. It includes the parametric effects from R-CLIPER plus those from shear and topography; each with their own equation. Lonfat et al. (2007) found that this model was an improvement over R-CLIPER forecasts. However, PHRaM was found not to produce the strong asymmetries associated with vertical shear. They conceded that many additional processes need to be included in the model such as convergence along a coastline, extratropical transition (ET), and moisture supply. The model we create considers these deficiencies by dividing the U.S. coastline into seven geographical regions (explained below). Southern regions have an inherent

abundance of moisture, whereas northern regions do not. Convergence along coastlines and possible ET also become apparent in our regional composites.

We encourage the interested reader to read about the Areal Tropical Rainfall Potential Technique (TRaP; Kidder et al. 2005) and its ensemble counterpart, eTRaP (Ebert et al. 2011). And for a historical perspective, the work of Schoner and Molansky (1956), Riehl and Malkus (1961), Simpson and Riehl (1981), the Kraft "Rule of Thumb," Schoner (1968), Goodyear (1968), Haggard et al. (1973), Griffith et al. (1978), Spayd and Scofield (1984), Pfost (2000), and Kidder et al. (2000).

2. 2. 3. Numerical weather prediction models

One of our primary research objectives (2 above) is to provide guidance on guidance (i.e., a forecast of a forecast) for GFS hurricane rainfall forecasts. With the power of numerical weather prediction (NWP) models, the need for analog and statistical techniques such as those described above may seem unnecessary. However, a NWP model's precipitation forecast is subject to the biases and deficiencies of the model. These deficiencies can result from improper initial and boundary conditions, parameterizations, and/or resolution, to name a few. Therefore, the creation of a statistical dataset such as ours allows for the recreation of simple, core methods in TC rainfall. The goal is to find explanations for discrepancies in rainfall forecasts.

When compared to the North American Mesoscale model (NAM; Janjic et al. 2005) and the Geophysical Fluid Dynamics Laboratory model (GFDL; Kurihara et al. 1995), Marchok et al. (2007) found that the GFS performed best in three categories: the ability to match QPF patterns, ability to match the mean value and volume of observed rainfall and reproduce the distribution of rain, and the ability to produce extreme rainfall amounts. Even though these models will be discontinued soon, or have already been discontinued, the work of Marchok et al. (2007) provides the basis for developing our analysis of GFS TC rainfall. Furthermore, the methods developed here can be used for future NWP models.

We seek to improve the performance of the GFS (or any NWP model with our methodology) by investigating those environments that are conducive to a good or bad GFS TC rainfall forecast.

3. Methodology

3. 1. Development of the Stage IV rainfall statistical dataset

Rainfall data for TCs were collected from 2004 – 2016. Best Track (BTK) storm data were collected from the revised Atlantic hurricane database (HRD, cited 2017). Automatic Tropical Cyclone Forecast (ATCF) files were used to identify GFS TCs. Six-hourly rainfall data were acquired from Stage IV (Lin and Mitchell 2005). These climatological rainfall grids are ingested into our statistical TC rainfall model (detailed below).

3. 1. 1. Aggregation of Stage IV rainfall data

To identify unique regional characteristics in TC rainfall, the U.S. coastline was separated into seven different geographical regions based on a cluster analysis of landfall locations from 2004 to 2012 (Fig. 1). Prior knowledge of TC storm track was used to help decide the locations of these regions. For example, storms in the Southern Texas region are translating east to west, whereas those in the Northern Gulf are primarily heading north and possibly recurving into the mid-latitude synoptic flow. Data were binned out to 500 km from storm center on an equidistant grid with a 10 × 10 km spacing for the years 2004 – 2012. This spacing was chosen so that regions with few 6-h TC fixes could have full coverage across the grid. At each grid point of the Stage IV dataset, a latitude/longitude pair was found, converted to a distance on an equidistant cylindrical grid, and placed in its respective bin for each region and a full U.S. composite.

Earth-, motion-, and shear-relative rainfall grids were created for the seven regions and the full U.S. composite. Motion was calculated as the storm's previous 6-h movement and bearing. A grid was projected on to the rainfall data and then rotated such that the rotated bearing and rainfall field pointed "up." For example, a storm moving to the northeast, with a previous 6-h bearing of 45° east of north, was rotated left 45°. An example of rotating a rainfall grid by several degrees is shown in Fig. 2.

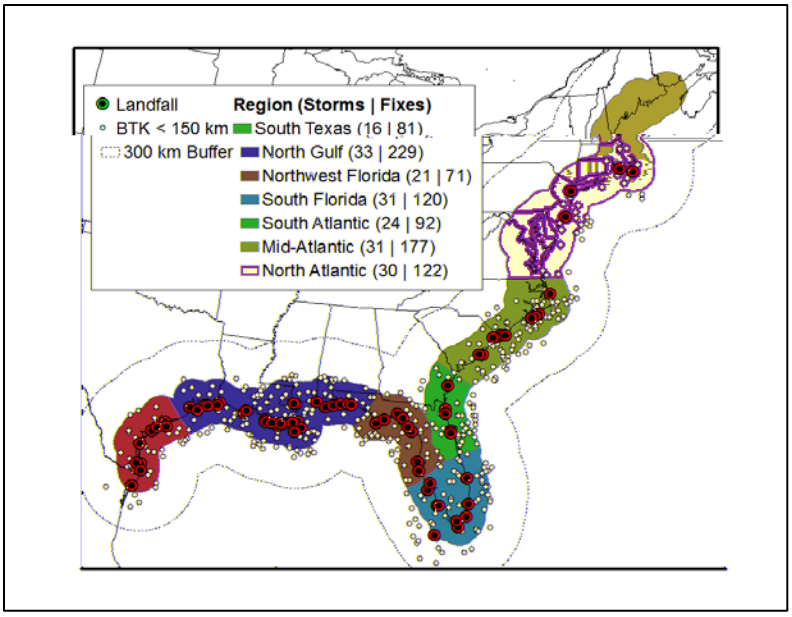

Fig. 1. The seven geographical regions. TC landfall locations are black/green dots for 2004 – 2012. Other 6-h locations within 150 km of the U.S. coast are shown for comparison.

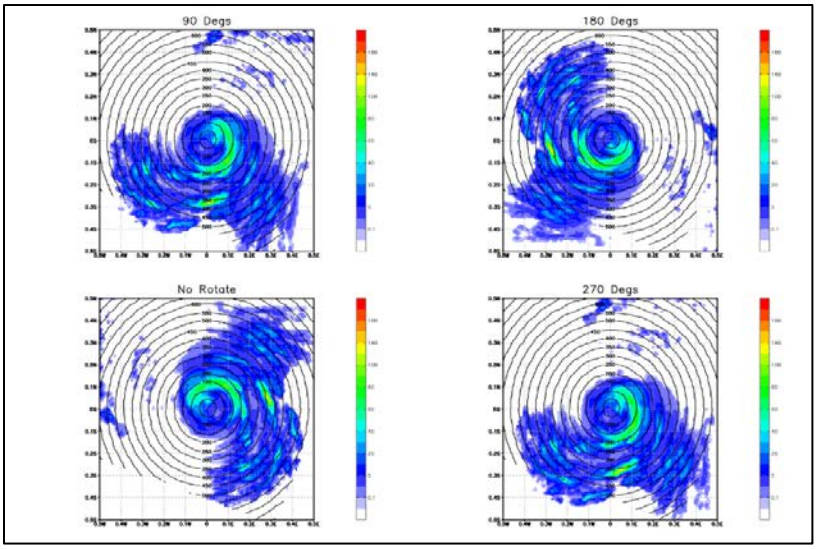

Fig. 2. Example of rotated grids binning technique.

Table 1. Intensity categories.

Category	Name	Wind Speed [kt]
TD0	Tropical Depressions	< 34
TS0	Weak Tropical Storms	34 - 45
TS1	Strong Tropical Storms	46 - 63
HU0	Weak Hurricanes	64 - 82
HU1	Strong Hurricanes	> 82

In addition to rotating the grids, each region and the U.S. composite were further composited based on individual storm intensity, shear magnitude, and storm speed. With regards to storm intensity, each region was categorized as either Tropical Depressions, Weak Tropical Storms, Strong Tropical Storms, Weak Hurricanes and Strong Hurricanes (Table 1). Unfortunately, this caused individual datasets within certain regions to have too few points to be statistically rigorous. Visual inspection of each region's intensity composites revealed that those intensity categories with similar rainfall structures and magnitudes within each respective region could be combined (discussed later). Figure 3 shows the combination of these intensity categories. Rainfall composites for shear categories (Low, < 5 m s^{-1}; Moderate, 5 – 10 m s^{-1}; and High > 10 m s^{-1}; Wingo and Cecil 2010) were prepared for each region and the entire U.S. Results from the shear categories then were combined like those for the intensity categories. This compositing methodology allows us to glean useful information about rainfall characteristics due to latitudinal or topographical differences between the seven geographical regions.

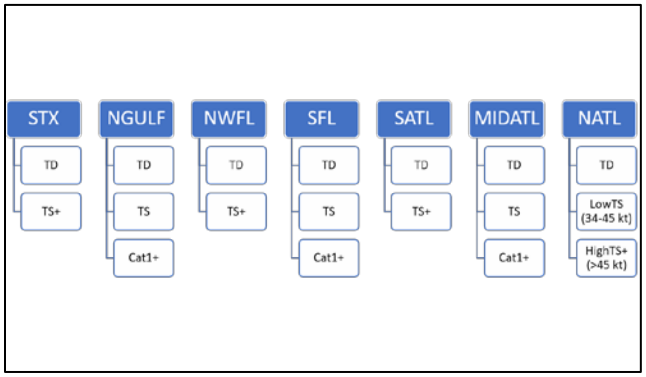

Fig. 3 Aggregation of intensity categories for each region.

3. 2. Development of statistical rainfall forecast model

To fulfill Research Objectives (1) and (3), we developed a statistical hurricane rainfall guidance product based on the datasets discussed above. The model can take any latitude/longitude pair, ingest a composite rainfall grid that corresponds to its shear, motion, intensity, and/or region, and place that rainfall grid on a global grid to accumulate rainfall for a 72-h forecast period. The model is like R-CLIPER and PHRaM in that it uses a climatological approach. However, it utilizes raw, frequentist statistics instead of parameterized methodologies. And, for the reasons stated above, we believe it can improve on baseline parameterized approaches to gain useful insight into TC rainfall forecasts.

Since the primary mechanism that orients TC rainfall is shear (when of sufficient strength; Chen et al. 2006; Reasor et al. 2013; Xu et al. 2014), the rainfall accumulation algorithm first uses the forecast shear magnitude and direction at the center of the TC. If the shear is too weak, the motion-relative dataset is used instead. And, if there is no previous 6-h motion (such as forecast hour 0), then the earth-relative dataset is used. This hierarchical approach is used at every 6-h timestep during the life of the forecast. As the storm progresses between regions (say, from Southern Florida to the Southern Atlantic) the algorithm uses the rainfall fields for the region in which the storm center is located. Rainfall is only accumulated out to 500 km from the storm center since the statistical datasets only extend to that distance. Finally, the shear- or motion-relative datasets are rotated by the 200 – 850 hPa shear vector or the previous 6-h motion vector such that the “up facing” dataset described above points in the direction of the vector that is used. For example, if a storm has a shear heading of 45^{o} east of north, the shear-relative dataset for the region in which the storm is located would be rotated 45^{o} east of north (like Fig. 2, but in the reverse and for a forecast). This ensures that key signatures are placed in climatologically correct locations with respect to the storm vector in question, such as a rainfall maximum in the DSL region of the forecast (if that is the regional characteristic).

3. 3. Development of a GFS TC rainfall skill regression model

We also created a regression model to produce a forecast of a forecast for GFS TC rainfall. For any GFS TC rainfall forecast, the equation can be applied to produce a predicted GFS TC rainfall skill score based on fractions skill score (FSS; defined below). Sixteen storm

parameters from the Statistical Hurricane Intensity Prediction System (SHIPS; DeMaria et al. 2005) were tested for the creation of the regression model. A stepwise regression technique was used to create a statistically-sound model of six parameters (out of the total of 16; Table 2) to regress against FSS. The resulting equation for forecasting the skill of a GFS forecast is:

$$FSS_i = 3.914 + 0.0031(D200) - 0.0011(DTL) - 0.0028(MSLP) + 0.0015(Z850) - 0.0064(SHRD) - 0.0101(RHLO). \quad (1)$$

Table 2. Description of SHIPS variables used in GFS FSS regression model.

SHIPS Variable ID	Name
D200	200 hPa Divergence
DTL	Distance to Land
MSLP	Mean Sea Level Pressure
Z850	850 hPa Relative Vorticity
SHRD	200 – 850 hPa Shear Magnitude
RHLO	Low-level Relative Humidity

4. Results

4. 1. Stage IV rainfall characteristics

To demonstrate the utility of using a decomposition of rainfall fields based on region, shear, motion, and storm intensity, we now highlight examples of regional characteristics that are important for this study of TC rainfall. Figures 4 – 6 show the full U.S. composite of rainfall for earth- and shear-relative approaches based on all shear magnitudes and those for the low (Fig. 4), moderate (Fig. 5), and high (Fig. 6) shear categories. Figure 7 shows locations of the 6-hourly fixes used. The geographical locations of the 6-hourly fixes are well dispersed along the U.S. Gulf and Atlantic coasts. It is well-documented (e.g., Black et al. 2002; Rogers 2003; Chen et al. 2006; Wingo and Cecil 2010; Reasor et al. 2013; Xu et al. 2014) that shear reorients the rainfall field and organizes rainfall in the DSL quadrant via the methods described above and within the cited research. However, the new and beneficial aspect of this study is that this type of analysis

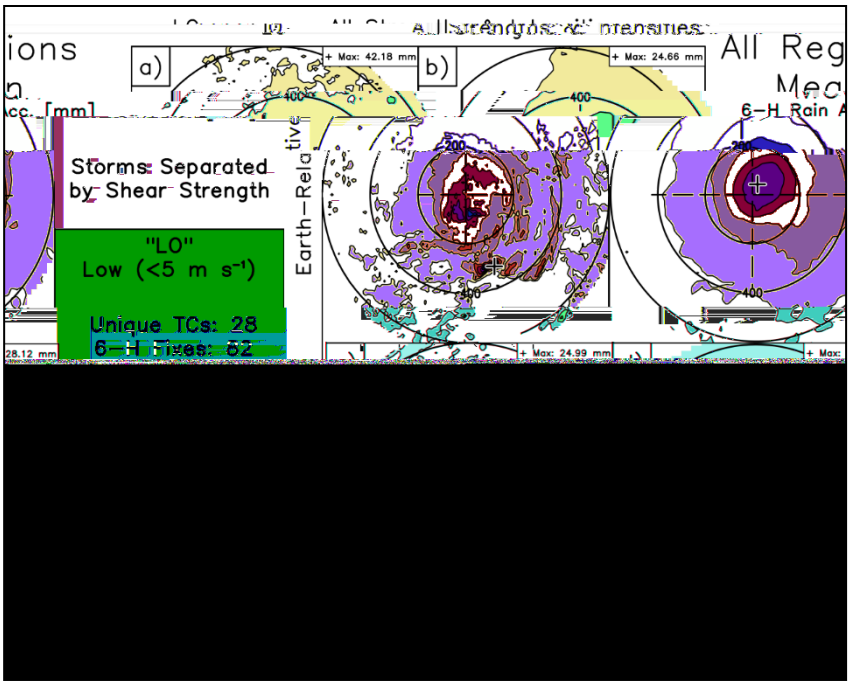

Fig. 4. Composite of Weak Shear (< 5 m s^{-1}) 6-h locations (a and c) and all strengths and intensities (b and d) in an earth-relative reference frame (a and b) and a shear-relative reference frame for the entire U.S. Six-hourly location density plot is on the bottom right. The composites for all strengths and intensities is shown for comparative purposes.

has never been performed using Stage IV data. The shear-relative "All Shears & Intensities" composites (Figs. 4d, 5d, and 6d), Stage IV rainfall data exhibit a DSL maximum that replicates previous findings. This confirmation between different datasets (satellite from previous studies and Stage IV from this study) is crucial to the ongoing research of TC rainfall.

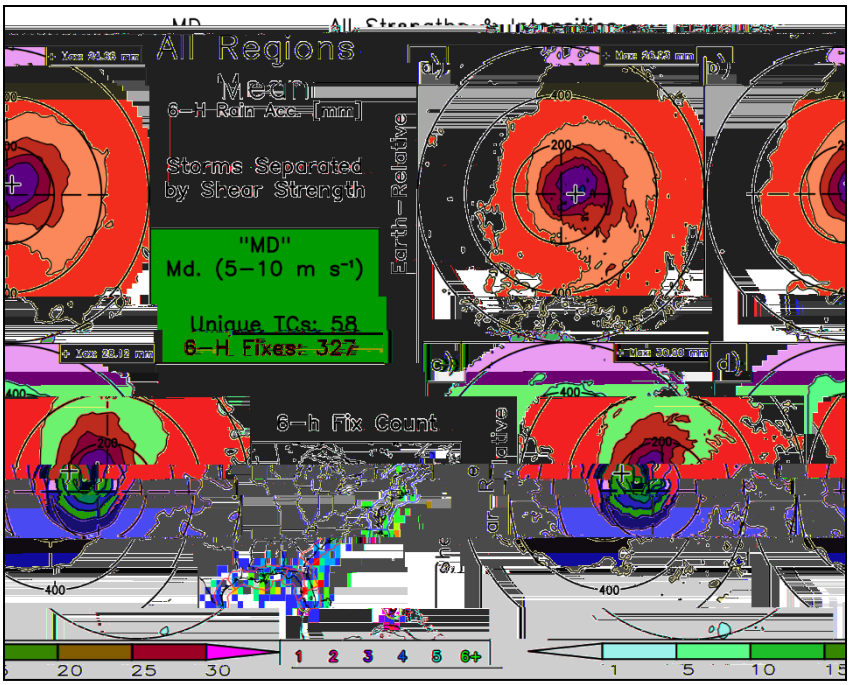

Fig. 5. As in Fig. 4, but for Moderate Shear (5 – 10 m s^{-1}).

As shear increases, its effects become more pronounced, and the composite storm rainfall fields become more asymmetric (Chen et al. 2006; Wingo and Cecil 2010). This can be seen in the low (Fig. 4), moderate (Fig. 5), and high (Fig. 6) shear-relative rainfall fields. The weak-shear, shear-relative rainfall field (Fig. 4c) is more symmetric than either the moderate- (Fig. 5c) or strong-shear (Fig. 6c) rainfall fields. The moderate- and strong-shear categories are similar in asymmetry; however, the strong-shear category has a more expansive rainfall field than the moderate- and weak-shear category. This can be related to findings by Lonfat et al. (2004) with respect to storm intensity. Specifically, as storm intensity increases, the radius of the peak azimuthal rainfall rate decreases (contracts). If we safely assume that strong-shear storms typically are of lower intensity and vice versa for weak-shear storms, then our findings coincide with those of Lonfat et al.

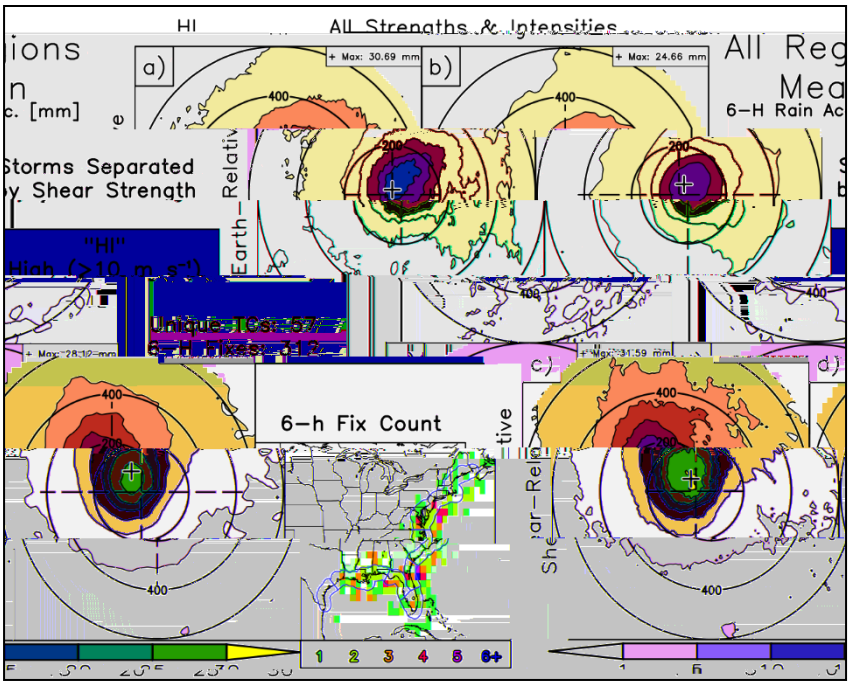

Fig. 6. As in Fig. 5, but for Strong Shear (> 10 m s^{-1}).

The importance of compositing our Stage IV rainfall data by shear magnitude is shown by comparing each of the low-, moderate-, and strong-shear categories, shear-relative (and, indeed, earth-relative) datasets with those from the “All Strengths & Intensities” (panels b and d in Figs. 4 – 6). Comparing those in the weak-shear category, we can see that the shear-relative rainfall (Fig. 4c) is more disorganized and more symmetric about the storm center than the full composite (Fig. 4d). This means that when we use this dataset (the shear-relative, weak-shear category) in our statistical forecast model (described below) we get a more representative forecast of storms within these shear criteria. This result coincides with Chen et al. (2006) where they found that the asymmetry decreases for weaker shear.

The importance of compositing the rainfall within a regional frame, and further compositing based on intensity is shown in Figs. 8 and 9 which show the TD intensity category for both the Southern and Northern Atlantic regions, respectively. The counts of TCs and 6-hourly fixes are nearly similar; however, the rainfall fields are different. The Northern Atlantic rainfall fields are more elongated and lighter in magnitude than the Southern Atlantic rainfall fields. This is indicative of the Northern Atlantic region having more stratiform rain due to a more baroclinic environment and/or interaction with a more sub-tropical synoptic-scale

environment. However, the primary mechanism which reorients rain (shear) is not lost in either of these regions' composites as both shear-relative composites exhibit DSL maxima (Figs. 7c and 8c).

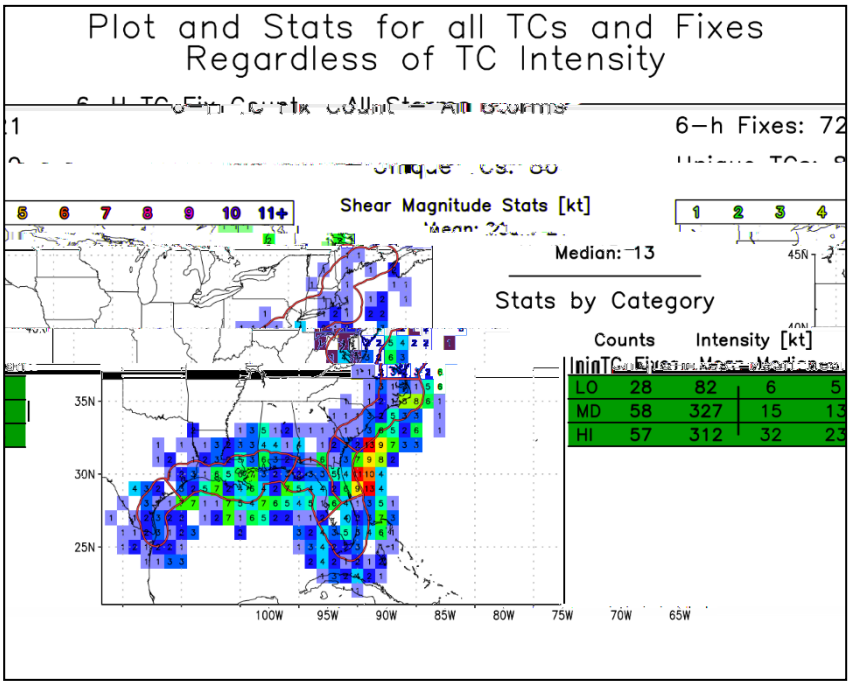

Fig. 7. Geographical density plot of 6-h locations for all storms within the developmental dataset.

The regional composite datasets are needed to understand TC rainfall structure. Previous studies have performed similar compositing, but with satellite data, and not in small-scale, regional domains like this study. The unique shear magnitude, storm motion, and storm intensity characteristics, combined with the rotation and alignment with respect to shear-, motion-, and earth-relative data frames have revealed important regional rainfall structures not previously seen from other studies. We are working to further document and detail these structures.

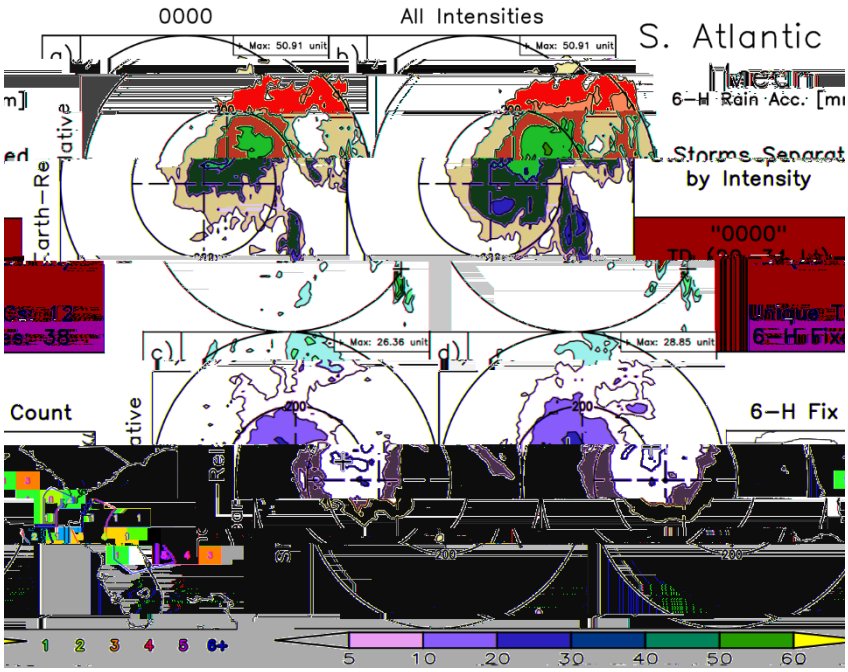

Fig. 8. Southern Atlantic regional composite of combined Intensity category "TD" (20 – 34 kt maximum sustained winds) 6-h locations (a and c) and all intensities (b and d) in an earth-relative reference frame (a and b) and a shear-relative reference frame. Six-hourly location density plot is on the bottom right.

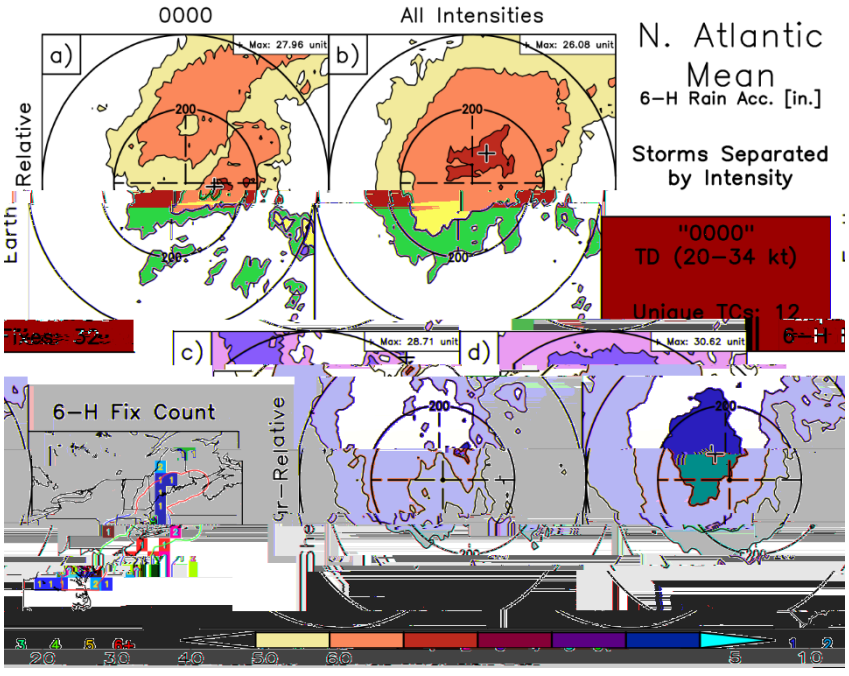

Fig. 9. As in Fig. 8, but for the Northern Atlantic region.

4. 2. A statistical rainfall model forecast

An example 72 h storm total rainfall forecast is given in Fig. 10 for TS Ana (2015) beginning at 0000 UTC 9 May 2015. The corresponding observations are shown in Fig. 11. The forecast shows that a simple statistical forecast model can provide a reasonably good forecast. The locations of maximum rainfall for the forecast and observations are collocated in southern NC with values of 8.65 in. and 7.61 in., respectively. The region of maximum rain was forecast for the southern SC/NC border and north through northeast NC. Both the observations and the forecast show a right of track maximum located along the NC coast. Due to the forecast model's hierarchical approach of selecting rainfall datasets based first on the shear magnitude, the accumulation of rainfall on land is due to the persistent northerly shear vector combined with the TC's slowing and turning to the northwest. This region's (MIDATL) shear-relative datasets based on shear magnitude (Fig. 12) have more of a general left-of-shear maximum in rainfall as opposed to a primary DSL in the full U.S. composite (Fig. 5d). Therefore, the accumulation of rain could occur mostly to the left of the track where the observationally large accumulations of rain occur.

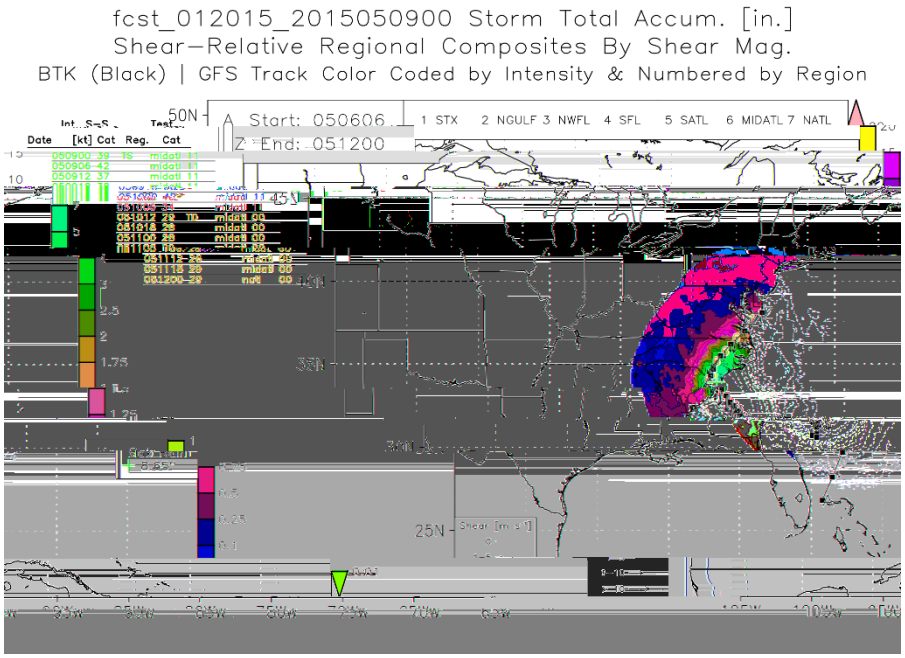

Fig. 10. TS Ana (2015) 72-h forecast from our model. Initialized at 0000 UTC 9 May 2015. Regions used within the forecast are indicated by numbers in the upper left table, while and the intensity is shown as a color. Best track storm path location is shown as a black track.

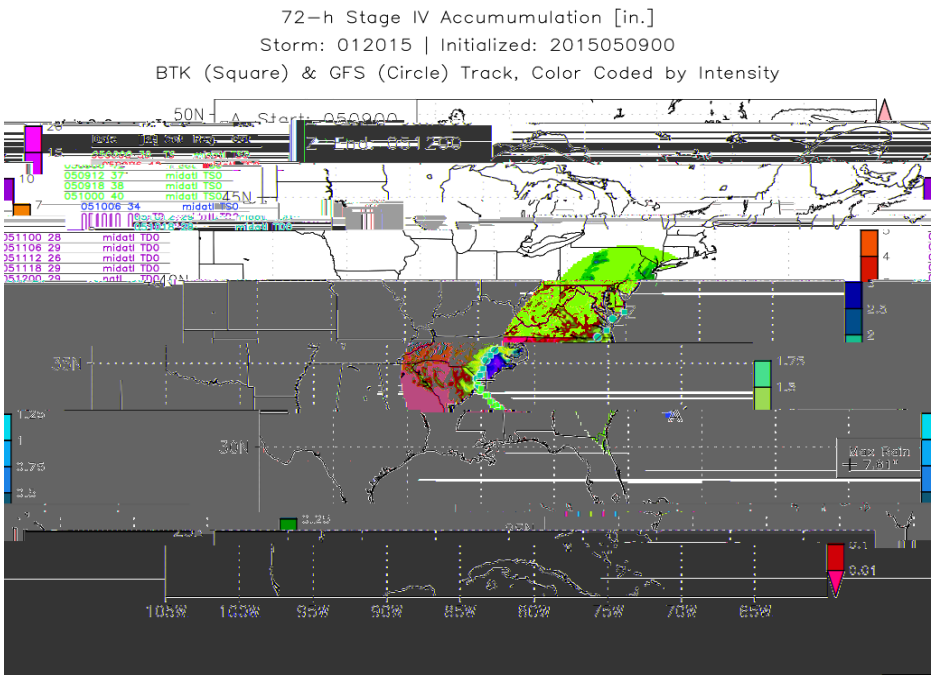

Fig. 11. Stage IV observations corresponding to the forecast in Fig. 10.

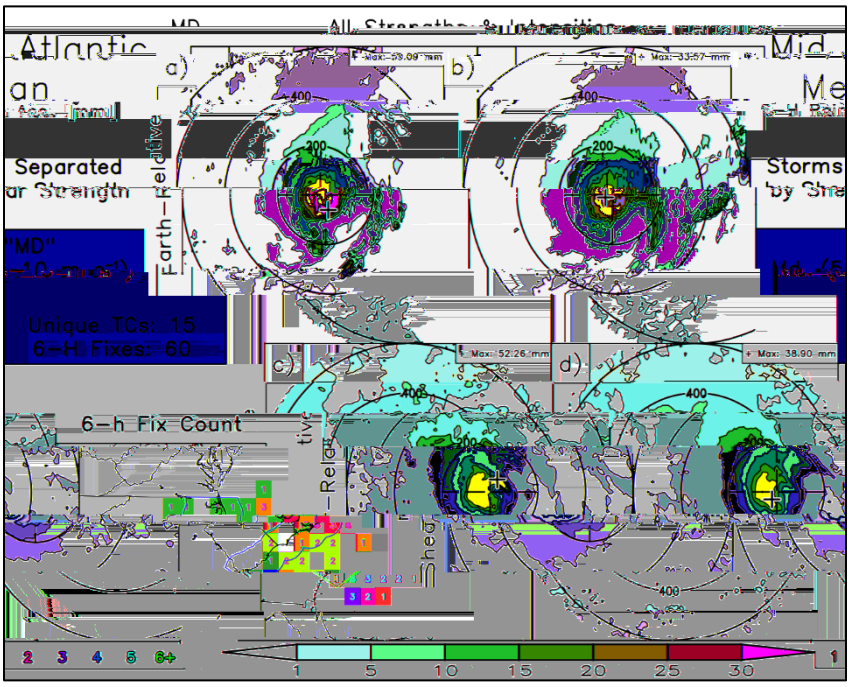

Fig. 12. As Fig.5, but for the Mid-Atlantic Region.

4. 3. GFS and our statistical model forecast skill

We wished to compute GFS TC rainfall skill. The methodology for this purpose is given in Section 3.3. Yearly reports on GFS performance (found at http://www.emc.ncep.noaa.gov/GFS/perf.php) do not provide a detailed analysis of TC rainfall alone, but for the entire CONUS on a seasonal basis. Another goal of our work was to provide this detailed analysis of GFS TC rainfall skill. In addition to the metrics used by EMC, we focus on fractions skill score (FSS; Roberts and Lean 2008).

Fractions skill score is becoming a popular metric for assessing the skill of rainfall forecasts (e.g., Marchand and Fuelberg 2014). Its "fuzzy" (Ebert 2008) verification approach permits minor deviations in the exact location of quantitative precipitation forecasts (QPFs). A radius of influence (ROI) is designated as a search radius around a grid point. If rainfall in a grid cell within the radius falls within the prescribed accumulation threshold, it is marked as a hit, and conversely a miss if not within the threshold. The grid point in question is then given a ratio of hits to total grid cells within the search radius. This procedure is done for the observational (Stage IV in this research) quantitative precipitation estimate (QPE) and the forecast (QPF) separately. The FSS is computed from these fractions. A score of 1 represents perfect skill, and 0 indicates no skill. The classical 2 × 2 contingency table (Wilks 2006) was used to compute biases and ETS.

4. 3. 1. GFS rainfall skill

Figure 13 shows GFS FSS for our full dataset (2004 – 2016), including all forecasts combined at all thresholds and radii of influence. As is expected, larger ROI exhibit better skill since the FSS can incorporate more grid points around the grid point in question to create a higher fraction. GFS skill decreases with increasing threshold. Overall, the GFS performs well for the thresholds shown here. The FSS does not fall below 0.5 for any ROI except at the 150-mm threshold with an ROI of 25 km. Bias and equitable threat score (ETS) are also displayed in Fig. 13. Overall, the GFS overestimates rainfall at thresholds less than 10 mm and underestimates for higher thresholds. The ETS ranges between 0.26 and 0.43.

To provide a comparison with EMC's annual CONUS reviews, Figure 14 shows average GFS TC ETS and bias computed for 2015 (the year of the most-recent available EMC review) and values for CONUS estimated from Yang (Cited 2017) during the JJA season. GFS TC

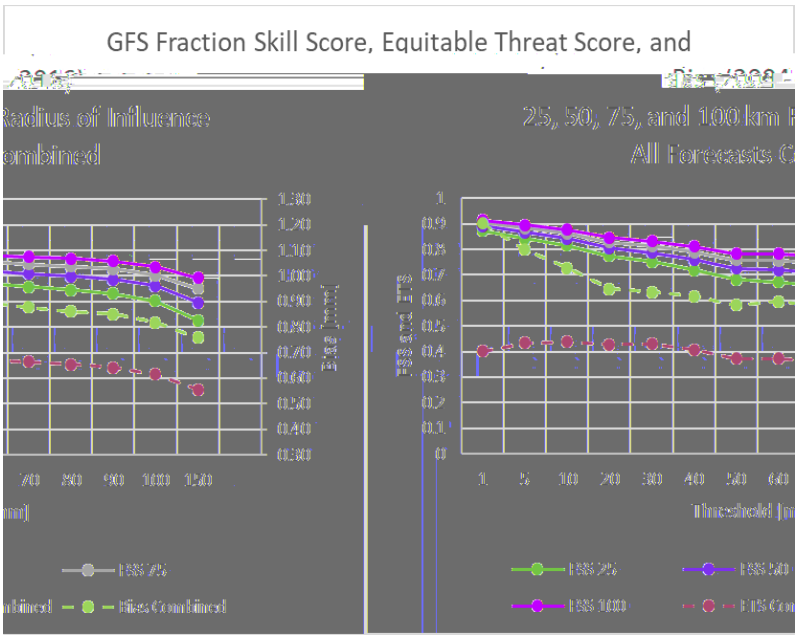

Fig. 13. GFS Fraction Skill Score, Equitable Threat Score, and Bias (2004 – 2016). All 72-h forecasts values (a, b, c, and d in a 2 × 2 contingency matrix) to compute the scores were combined. For example, all the a, b, c, and d values from a 2 × 2 contingency matrix were summed at each threshold, and scores were computed from that summation.

rainfall skill (ETS) is less than that over the entire CONUS at thresholds less than 20 mm. Between 20 mm and 70 mm, GFS TC rainfall skill is more than the entire CONUS skill. This indicates that at lower thresholds (< 20 mm), the GFS has a harder time forecasting TC rainfall than all rainfall in the entire CONUS, and at thresholds between 20 and 70 mm, GFS TC forecasts are more skillful. We cannot determine the relationship for thresholds greater than 80 mm, but at 80 mm, GFS TC rainfall skill is less than that of the CONUS.

The GFS on a CONUS-wide scale ranges between approximately 0.7 and 1.3 (Fig. 14). However, the GFS TC bias ranges from 1.3 at a 1 mm threshold to 0.1 at 150 mm. Stated simply, GFS TC rainfall amounts are over-forecast at lower thresholds (< 10 mm) and under-forecast at greater thresholds. At smaller thresholds (less than 10 mm), GFS TC rainfall bias is similar to the CONUS bias except less than 5 mm where the CONUS bias is greater. This indicates that light TC rainfall is over-forecast. And, at all other thresholds (> 10 mm), GFS TC rainfall under-forecasts. This means that GFS TC rainfall forecasts will underestimate large-threshold rain events.

Our analysis, which specifically investigates GFS TC rainfall skill, is valuable in that it does not include any other effects which affect overall GFS rainfall skill (e.g., synoptic-scale rain showers, frontal zones, or summer time convective events). It is purely TC-centric. These differences in GFS rainfall performance are crucial to understanding GFS TC rainfall forecasts. It is not safe to assume that if the GFS does well on a CONUS-wide scale during JJA, that it will perform equally well on a TC-sized scale. These results show that, on average, GFS TC rainfall skill differs from that of the entire CONUS.

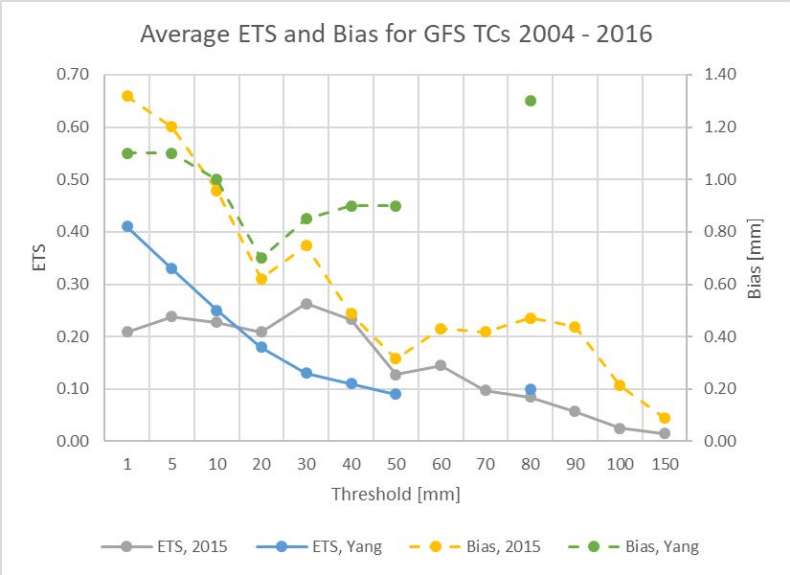

Fig. 14. ETS and Bias computed for CONUS (Yang, Cited 2017; labeled "Yang") and only for TCs (labeled "2015"). Yang ETS and Bias are for JJA during 2015 for CONUS.

4. 3. 2. Skill of our TC rainfall model

The skill scores of our statistical rainfall model were analyzed similar to that done for the GFS (previous section). The 2004 to 2016 dataset was separated into developmental (2004 – 2012) and test (2013 – 2016) datasets. The Stage IV statistical composite grids described earlier are those used for the developmental dataset. These 2004 – 2012 datasets are the datasets used in creating our model's QPFs for the 2013 – 2016 forecasts.

Our TC rainfall model's forecast skill (FSS and ETS) and bias are shown in Fig. 15. In terms of FSS, the model performs well (≥ 0.5 FSS) up to the 50-mm threshold for all ROI greater than 25 km. As the threshold increases, FSS diminishes near to zero. This is expected since the model is built on the statistical aggregation of rainfall, and it accumulates these datasets (e.g.,

Figs. 4 – 6, 8 – 9, or 12) on a 6-hourly basis. Therefore, if we are trying to forecast 150 mm of rain with the U.S. composite with a shear-relative dataset, we use Fig. 4c. If we assume that 1) the forecast storm does not change regions or shear magnitudes, 2) the storm stays at one latitude/longitude pair, and 3) shear direction does not change, it would take six, 6-hourly time steps to accumulate 150 mm of rain at the location of maximum rainfall on a forecast grid that corresponds to the location in Fig. 4c. Since our model is a mean of each region and the regions' various storm-parameters, it is more likely to accumulate rain more accurately for those storms with less-extreme rainfall (or, more normal rainfall).

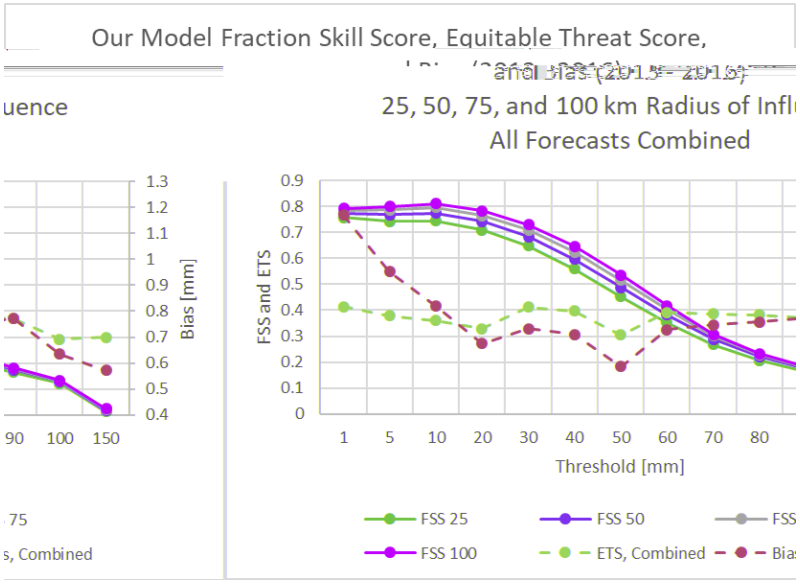

Fig. 15. As in Fig. 13, but for our TC model.

The ETS for our model (Fig. 15) ranges between 0.3 and just above 0.4, depending on rainfall threshold. This shows the utility of the fuzzy verification methodology. On a grid-cell-by-grid-cell basis, our model exhibits mediocre performance. However, when incorporating a search radius as in the FSS method, it performs much better. This approach is preferred, not in the sense that it gives our model a better score, but that it allows for slight variations in precise rainfall location. We believe it is fairer to assess model performance in this manner.

4. 3. 3. Comparing the GFS and Our Model

We compared the FSS of our statistical model to that of the GFS. Figure 16 shows FSS for both the GFS and our model at the 50 km ROI. For thresholds less than 40 mm, our model and GFS perform relatively similarly. However, for thresholds greater than 50 mm, the FSS of

the GFS and our model diverge, with the GFS considerably outperforming our model. This is expected since our model is a climatological model while the GFS is a fully-developed NWP model.

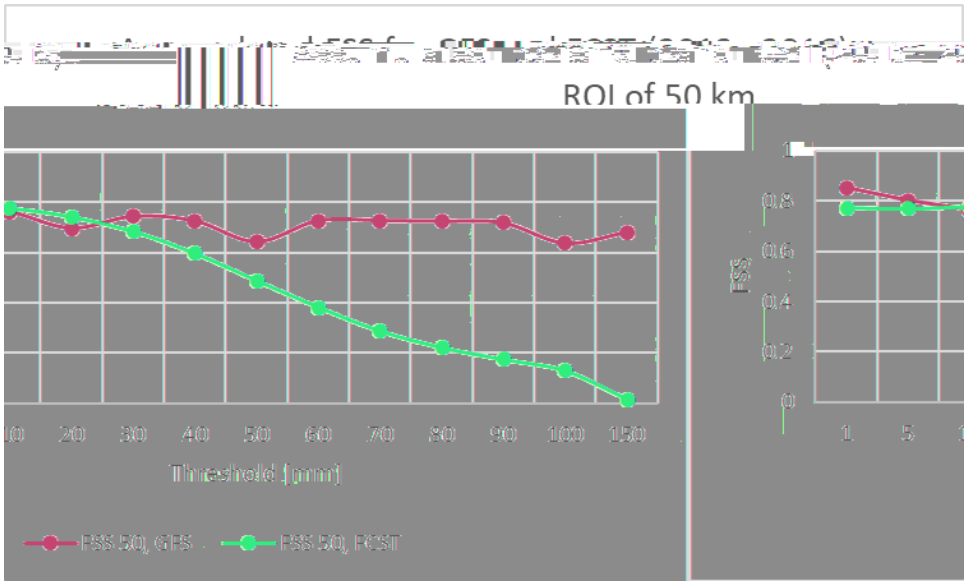

Fig. 16. Accumulated FSS for GFS and our model, 2013 – 2016.

Although the results of Fig. 16 were disappointing, Fig. 17 reveals a promising finding in favor of our model's performance. This figure shows the win percentage of our model and the GFS at the 50 km ROI at each rainfall threshold. For each forecast in the 2013 – 2016 dataset the FSS was compared between our model and the GFS. The win percentage is the percentage of forecasts with a higher FSS between both models. For example, with a sample size of 10 forecasts, if the GFS had a higher FSS on 3 of them, and our model on 7, the win percentages for the GFS and our model are 30% and 70%, respectively. Results show that our model beats the GFS on many occasions at varying thresholds. For example, our model outperforms the GFS nearly 65% of the time at the 20-mm threshold, and 54% of the time at the 90-mm threshold.

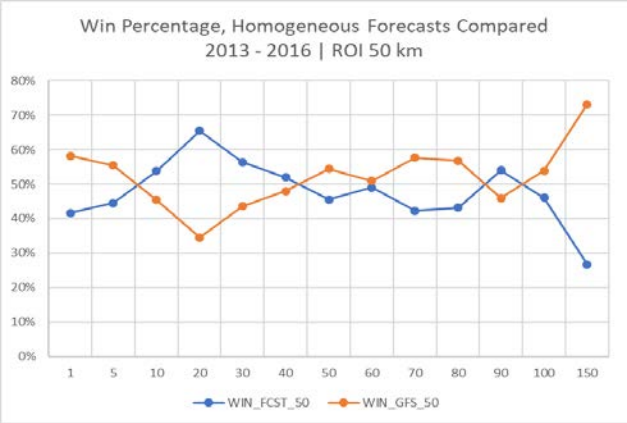

Fig. 17. Percentage of wins at each threshold for each model.

While we cannot expect our TC rainfall model to beat the GFS all the time, the previous results show that it can outperform *some* of the time. The logical questions following these results are “why, and can we predict when?” Figure 17 shows a scatterplot of GFS FSS and our model’s FSS at the 50-mm threshold with an ROI of 50 km. There is a positive relationship between GFS FSS and our model FSS indicating that if the GFS is going to perform well, then our model most likely will as well. To answer the question of “when will the GF perform well?” we investigated whether there were GFS environments that were conducive to good or bad forecasts. That is the topic of the next section.

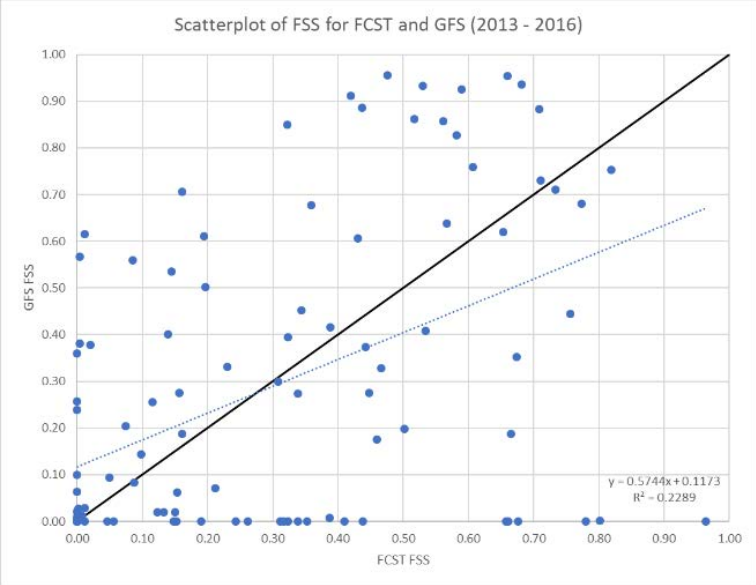

Fig. 18. Scatterplot of FSS for our model FSS and the GFS FSS. A one-to-one line is shown in black. The blue dashed line is the linear relationship between our model's FSS and the GFS's. Equation and variance explained are in the bottom right.

4. 4. Prediction of GFS TC rainfall skill

The natural progression of our work after analyzing GFS TC rainfall skill, was to find those instances when the GFS performs well or poorly, and qualitatively investigate whether there are meteorological parameters that can predict whether a GFS forecast would be good or bad. Similarly, can we do the same analysis with our model? Our research has not reached the point where we can describe those meteorological conditions favorable for a good or bad forecast using our model, but we have investigated those meteorological conditions for the GFS. The assessment of our model will be concluded in Tristan Hall's dissertation, along with a more-extensive investigation of the GFS.

The GFS forecast dataset was separated into "Top, Middle, and Bottom" categories based on FSS. The Top category were those forecasts whose FSS was greater than 0.66; the Bottom, less than 0.33; and Middle, everything in between. The Middle category served as a "sanity check" to ensure that differing environments did exist between the Top and Bottom categories. In other words, if Top and Bottom forecasts occur in greatly different environments, Middle should be between them. Mean environmental values were computed at each forecast hour for the forecasts belonging in the Top, Middle, and Bottom categories.

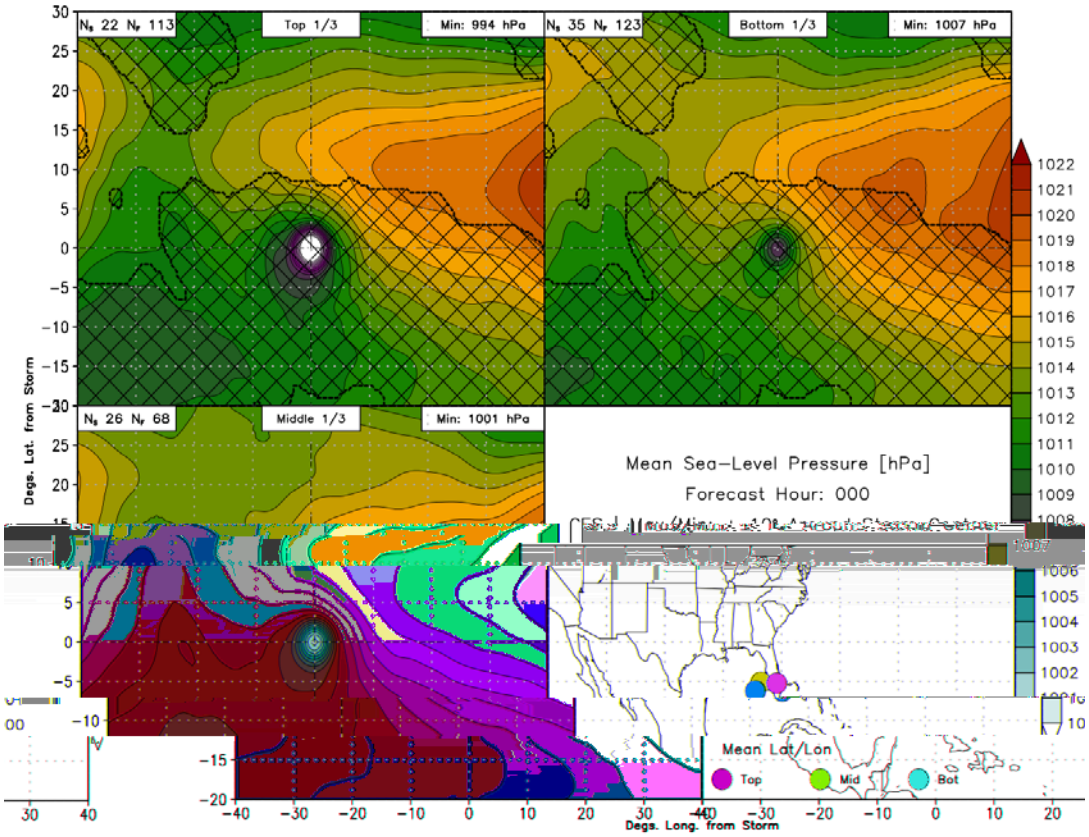

Fig. 19. Mean seal level pressure [hPa] at forecast hour 0 for Top, Middle, and Bottom ranked GFS forecasts based on FSS. Mean geographical location of each category is shown in the bottom right.

The first meteorological variable we investigated was MSLP at the time of GFS initialization (Fig. 19). Hatched areas in the figures indicate regions that are significantly different ($p \leq 0.05$) between the Top and Bottom forecast categories. A clear difference between the Top and Bottom forecasts is that the Top forecasts consist of relatively stronger (lower pressure) storms than the Bottom forecasts. To test correlations between storm parameters and environmental conditions, variables from the SHIPS dataset were used and correlated against FSS. For example, if we wanted to correlate MSLP and FSS, each forecast's MSLPs and FSSs were used together for the entire dataset to create the statistic. Results show a -0.28 statistically significant correlation between FSS and SHIPS MSLP. This correlation indicates that the lower the MSLP, the higher the FSS. Why the GFS performs better for more-intense storms is still under investigation. Perhaps it is because the GFS can organize rainfall better for stronger TCs. As storm intensity increases, rainfall asymmetry decreases (Xu et al. 2014), and the radius of

maximum rain decreases (Lonfat et al. 2004). It may be possible that the GFS can better handle this type of TC rainfall organization based on intensity. These questions will be answered in Tristan's dissertation.

Further inspection of Fig. 19 shows that the sub-tropical ridge influences the skill of the GFS forecasts. The Bottom ranked forecasts occur with a stronger sub-tropical ridge than the Top forecasts. The location of the composited forecasts is not the cause of this difference since the bottom right panel shows that there is only an approximately three-degree difference in longitude between the Bottom and Top forecasts. Thus, if either the Top or Bottom forecasts were shifted to the east or west, it would not explain the difference in sub-tropical strength to the east of the storm. To test the correlation between FSS and the strength of the sub-tropical ridge, a box was superimposed over the climatological location of the sub-tropical high over the Atlantic Ocean (between 25^{o} N and 45^{o} N and 20^{o} W and 55^{o} W). The climatological location of the sub-tropical high was determined by compositing MSLP for all months from 2004 – 2016 (not shown). Areal maximum and average MSLP values were calculated for each 72-h forecast. There is a -0.02 statistically insignificant correlation between FSS and both areal maximum and average MSLP over the climatological sub-tropical high region for all forecasts in our test dataset. However, for forecasts occurring during July and August, there are statistically significant correlations between the forecast areal-average (in the box described above) sub-tropical high strength and FSS of 0.35 and 0.30, respectively. During these months, when the hurricane season is well-underway, a relatively strong sub-tropical high will lead to higher FSS.

The strength of the sub-tropical high also can be a proxy for other mechanisms that influence the storm. For example, deep layer steering flow is crucial to TC track forecasts (George and Gray 1976; Elsberry 1995). If the sub-tropical high were to become stronger, the pressure gradient between it and the tropics would increase, increasing the steering-level flow and therefore the translational speed of the TC. A statistically insignificant correlation of -0.05 is found between the previous 6-h speed and FSS for all forecasts in our test dataset. However, as was seen in the sub-tropical high strength discussion above, a statistically significant correlation of -0.34 and -0.30 exists between FSS and previous 6-h speed during the months of July and August, respectively. A reduction in strength of the sub-tropical high (and therefore a possible reduction in the gradient between the tropics and the sub-tropics) can cause a reduction in TC

forward speed. If that is the case, then a reduction in previous 6-h TC motion leads to an increase in FSS.

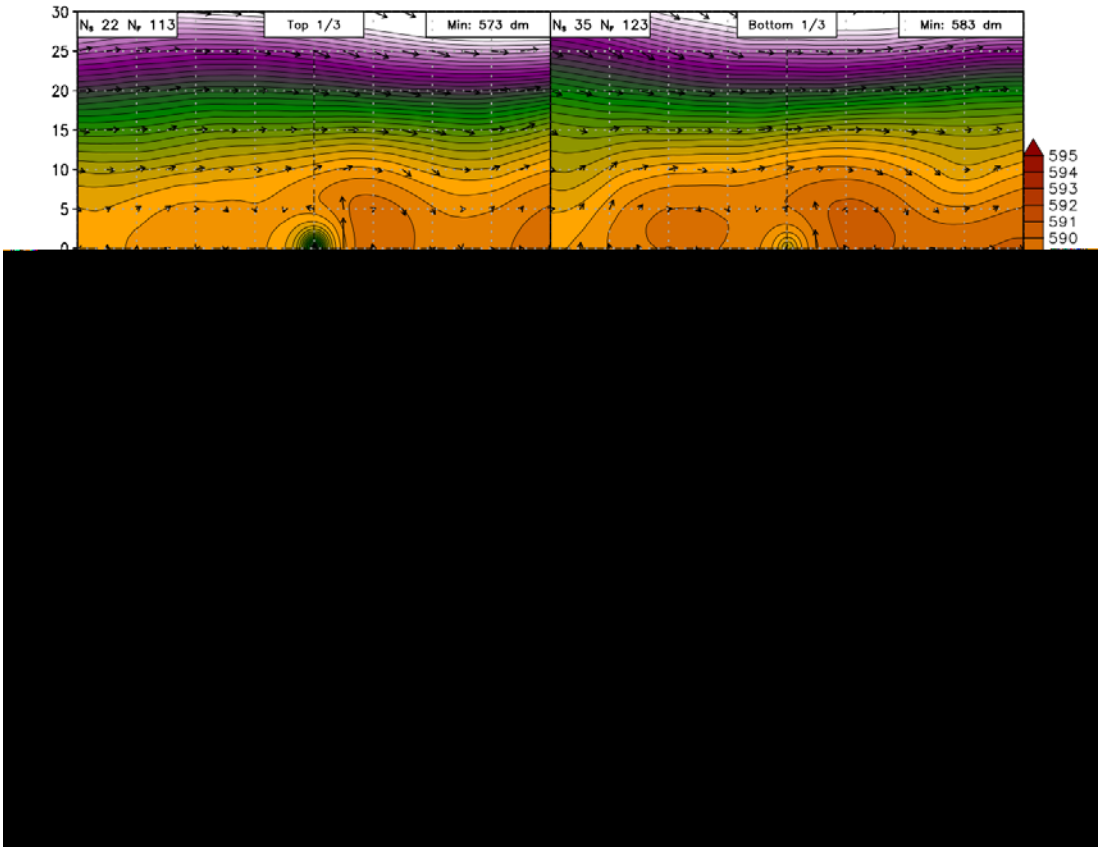

Fig. 20. As in Fig. 19, but 500 hPa Heights.

Looking higher in the atmosphere, Fig. 20 shows mean 500 hPa heights for Top, Middle, and Bottom forecasts at the time of GFS initialization. As observed with mean sea level pressure, the Top forecasts are associated with lower heights of the 500 hPa surface near storm center than the Bottom forecasts. The plots show that at GFS forecast initialization, both Top and Bottom forecasts are, on average, embedded within a mid-level ridge. However, the Top forecasts exhibit a weaker mid-level ridge to the west than the Bottom forecasts, which might explain their stronger intensity and greater FSS. By forecast hour 72 (Fig. 21), both Top and Bottom forecasts are located on the northwest side of a mid-level ridge. The Top forecasts are larger in areal extent with a deeper trough to their west than the Bottom forecasts. With the Top forecasts, the TCs appear to be interacting with an existing trough since approximately 25 degrees to the west there is a shortwave ridge. Looking at the Bottom forecasts, there is a considerably different trough

interaction to the west compared to the Top forecasts. The trough in the Bottom forecasts expands farther west and its axis farther west than the Top's. The downstream ridge in the Bottom forecast is stronger than the Top, indicative of an environment that is more baroclinic and related to possible Extratropical Transition (ET; e.g., Atallah and Bosart 2003; Abraham et al. 2004; Atallah et al. 2007). However, the extent to which ET may or may not be a factor has not been investigated yet. Finally, of note, there are no statistically significant differences in the mean heights between the Top and Bottom forecasts in Figs. 17 and 18. This is not to say that the patterns are insignificant, just that the values between the two plots are statistically similar.

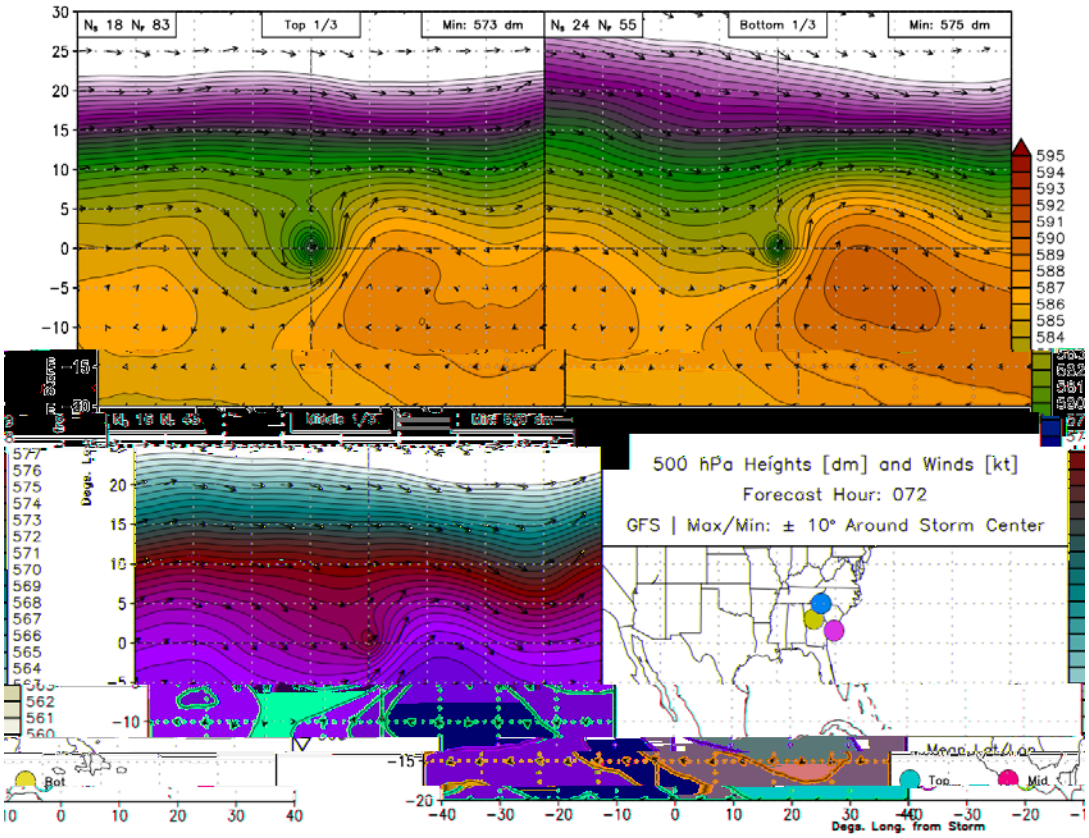

Fig. 21. As in Fig. 20, but at forecast hour 72.

To investigate the influence of an approaching trough and any subsequent baroclinic interaction, Fig. 22 shows 1000 – 500 hPa mean thickness anomalies at forecast hour 0. The anomalies are calculated from 2004 – 2013 monthly means. The strength of thickness associated with TCs in the Top forecast category is apparent, and its overall size is much larger in areal extent than the Bottom counterpart. Twenty degrees to the north and west, greatly different

environments are apparent: The top forecasts are within an anomalously larger thickness environment, whereas the Bottom forecasts are within an anomalously less thick environment. However, as forecast hour increases to 72 hours (Fig. 23), the region of greater thickness in the Top forecasts has moved east and is now situated northeast of the TC. The anomalous thickness trough to the northwest of the Bottom forecasts has shifted south and is now much closer to the TC, spanning from the west to the northwest of the TC within 15 degrees of the storm. This means that by forecast hour 72, a deep, anomalous trough is interacting, or will interact soon, with the Bottom forecasts' TC. This would result in an increased baroclinic environment for the TC, including increased vertical shear and possibly cold-core processes. Conversely, the Top forecast TCs' environment has not changed as much as the Bottom forecasts'. There is a minor thickness trough to the immediate west, but nothing as intense as what is seen in the Bottom forecasts.

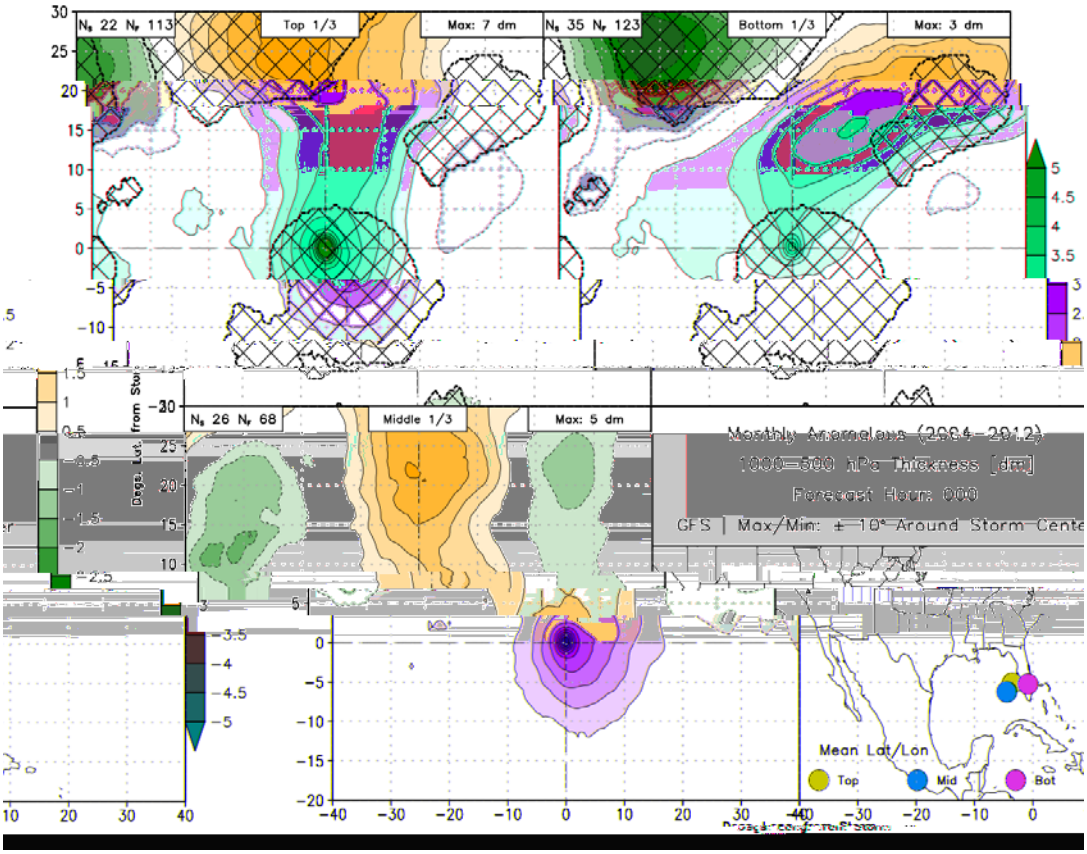

Fig. 22. As in Fig 19, but for anomalous 1000 – 500 hPa thickness at forecast hour 0.

A thorough analysis of contrasting moisture environments for the Top and Bottom forecasts remains to be done. For example, we need to investigate the relationship of low-level relative humidity (e.g., Elsberry 1995) and GFS performance.

Based on the investigation above, we summarize that the Bottom forecasts are TCs that are interacting with a sub-tropical, mid-level ridge and thickness gradient. This can result in an increased baroclinic environment for the TC, which results in increased shear, and more-complex rain fields. As the TC weakens in intensity, its climatological rainfall signature becomes increasingly more asymmetric and expansive. Similarly, as shear increases, the climatological organization of rainfall concentrates in the DSL quadrant. The GFS must simulate these intricacies to produce quality rainfall forecasts.

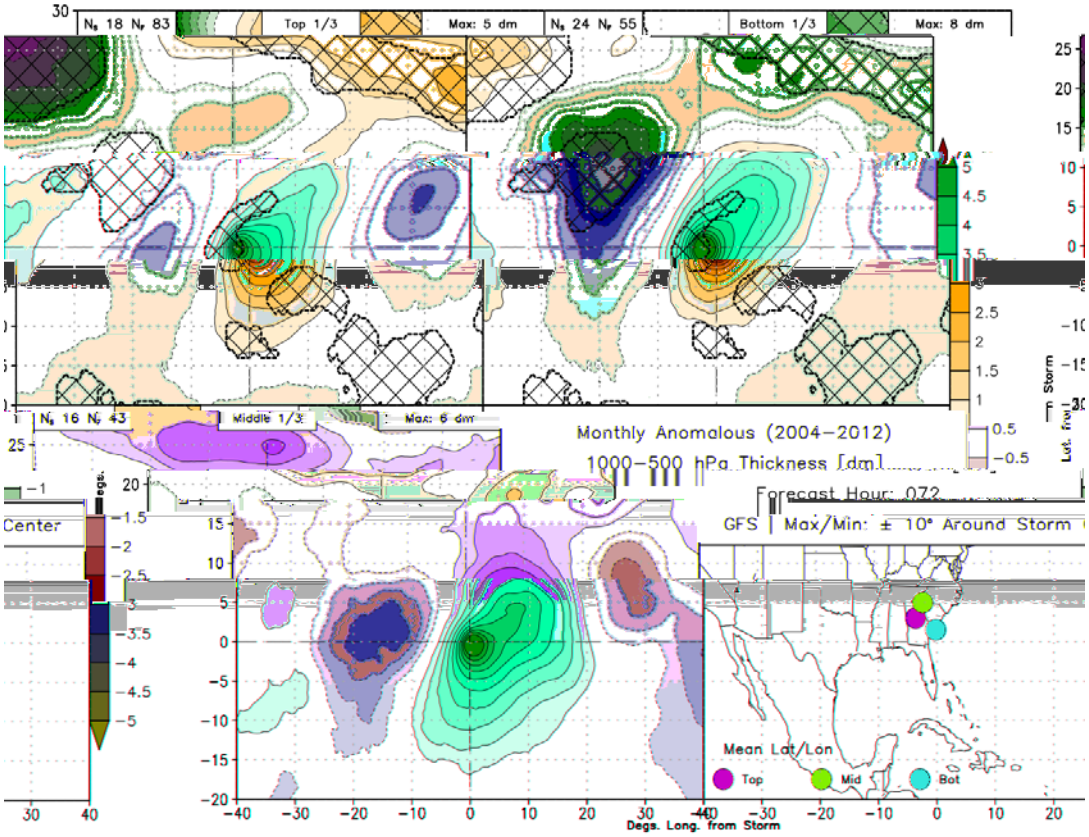

Fig. 23. As in Fig. 22, but for forecast hour 72.

4. 5. GFS regression model

To assess performance of the GFS FSS regression model (Equation 1 above), we computed a skill score (SS_{clim}) based on climatological values of the predictand's FSS for the

developmental dataset (Wilks 2006). The score indicates whether the regression model improves on climatology. The regression model exhibited an MAE of 0.197, an RMSE of 0.261, an explained variance of 0.352, and a SS_{clim} of 34%. An MAE is 0.197 means that, on average, the error in a forecast spans 40% of the allowable predicted skill. For example, if we predict an FSS of 0.5, the skill can range from 0.3 to 0.7. This is not ideal since we hoped for an MAE of less than 0.1. However, the model is a 34% improvement on climatology (SS_{clim}). This means that 34% of the time, it can beat the climatological forecast (which is just the mean of the developmental FSS). Again, this is not ideal, but it is interesting that we have developed the basis for a model which can predict GFS TC rainfall forecast skill.

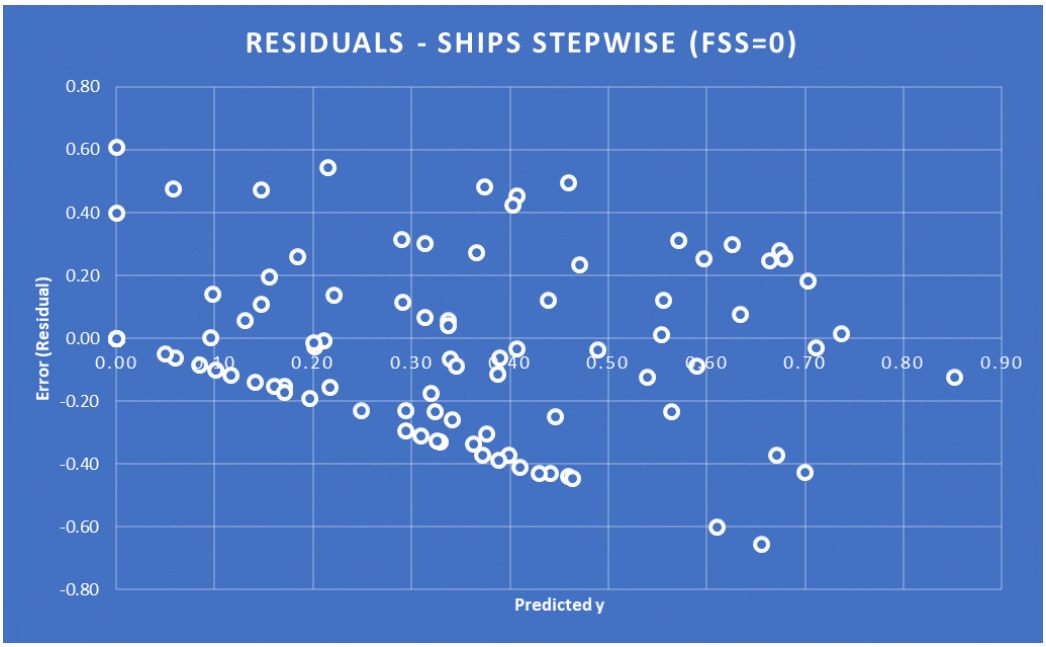

Fig. 24. Residual analysis of predicted y values (FSS).

Residuals for the GFS FSS regression model are shown in Fig. 24. There is appreciable scatter across the predicted *y* range. However, the residuals exhibit a negative slope. Therefore, if we use this model, a forecast with a small FSS is likely an under-forecast of skill (e.g., the skill is likely higher), and a forecast with a larger FSS is likely an over-forecast of skill (e.g., the skill is likely lower). Readers should note that we defined the residual, to be consistent with statistical error analyses, as Observations minus Predicted, which is opposite that of forecast error analyses in the atmospheric sciences, where observations are subtracted from the predicted variable. This regression approach may yet still have merit, and we are working on a further analysis of this

model. By the conclusion of Tristan's dissertation, we should have a full understanding of this model's skill and ability.

5. Conferences and Presentations

Some of the topics discussed above were presented by Tristan at the 96th Annual Meeting of the American Meteorological Society (AMS). Here is the link to the recorded presentation: https://ams.confex.com/ams/96Annual/webprogram/Paper285918.html.

Tristan also presented at the 32nd Conference on Hurricanes and Tropical Meteorology. The link to the recorded presentation can be found here: https://ams.confex.com/ams/32Hurr/webprogram/Paper293505.html.

6. Summary

We have analyzed TC rainfall structure along the U.S. East and Gulf Coasts using Stage IV data. We also created our own statistical rainfall forecast guidance product based on the Stage IV climatology. Our model performs well under ordinary circumstances since it is a climatological model. Further analysis is being conducted to determine those environments in which our model is expected to produce a good forecast. We also will use our model to discover any discrepancies in GFS TC rainfall forecasts. For example, if we look at a forecast from our statistical rainfall model and the GFS and we see similarities between rainfall structures, we can safely assume those structures in the GFS forecast are due to those variables used in our model (e.g., shear or motion). Therefore, discrepancies between the two models' forecasts are due to different factors than those used in our model.

Overall, GFS TC rainfall forecasts have less skill than CONUS-wide forecasts. However, the GFS still performs reasonably well. The purpose of this work is to identify when the GFS will perform well or poorly. We have investigated numerous meteorological conditions that could lead to good or bad GFS forecasts. We are still analyzing TC rainfall and TC rainfall forecast methods. Although it is a complex problem, we feel we have the right methods to improve TC rainfall forecasts. We have provided evidence of environments which are conducive to good or bad GFS TC rainfall forecasts, and these methods will be expanded and concluded in Tristan's Ph.D. dissertation.

7. Bibliography

Abraham, J., J. W. Strapp, C. Fogarty, and M. Wolde, 2004: Extratropical transition of Hurricane Michael: An aircraft investigation. Bull. Amer. Meteor. Soc., 85, 1323–1339.

Atallah, E., L. F. Bosart, and A. R. Aiyyer, 2007: Precipitation distribution associated with landfalling tropical cyclones over the Eastern United States. *Mon. Wea. Rev.*, **135**, 2185, doi:10.1175/MWR3382.1.

Atallah, E. H., and L. F. Bosart, 2003: The extratropical transition and precipitation distribution of Hurricane Floyd (1999). *Mon. Wea. Rev.*, **131**, 1063, doi:10.1175/1520-0493(2003)131h1063:TETAPDi2.0.CO;2.

Bender, M. A., 1997: The effect of relative flow on the asymmetric structure in the interior of hurricanes. *J. Atmos. Sci*, **54**, 703–724, doi:10.1175/1520-0469(1997)054h0703: TEORFOi2.0.CO;2.

Black, M. L., J. F. Gamache, F. D. Marks, C. E. Samsury, and H. E. Willoughby, 2002: Eastern Pacific Hurricanes Jimena of 1991 and Olivia of 1994: The effect of vertical shear on structure and intensity. *Mon. Wea. Rev.*, **130**, 2291, doi: 10.1175/1520-0493(2002)130h2291:EPHJOAi2.0.CO;2.

Chen, S. S., J. A. Knaff, and F. D. Marks, 2006: Effects of vertical wind shear and storm motion on tropical cyclone rainfall asymmetries deduced from TRMM. *Mon. Wea. Rev.*, **134**, 3190, doi:10.1175/MWR3245.1.

Corbosiero, K. L., and J. Molinari, 2003: The relationship between storm motion, vertical wind shear, and convective asymmetries in tropical cyclones. *J. Atmos. Sci.*, **60**, 366– 376, doi:10.1175/1520-0469(2003)060h0366:TRBSMVi2.0.CO;2.

DeMaria, M., M. Mainelli, L. K. Shay, J. A. Knaff, and J. Kaplan, 2005: Further improvements to the Statistical Hurricane Intensity Prediction Scheme (SHIPS). Weather and Forecasting, 20 (4), 531{543.

Ebert, E. E., 2008: Fuzzy verification of high resolution gridded forecasts: A review and proposed framework. Meteor. Appl., 15, 51–64.

Ebert, E. E., M. Turk, S. J. Kusselson, J. Yang, M. Seybold, P. R. Keehn, and R. J. Kuligowski, 2011: Ensemble tropical rainfall potential (eTRaP) forecasts. *Wea. Forecasting*, **26**, 213–224, doi:10.1175/2010WAF2222443.1.

Elsberry, R. L., 1995: *Global Perspectives on Tropical Cyclones*. Secretariat of the World Meteorological Organization, 289 pp.

Ferraro, R., and Coauthors, 2005: The tropical rainfall potential (TRaP) technique. part ii: Validation. *Wea. Forecasting*, **20**, 465, doi:10.1175/WAF861.1.

Frank, W. M., and E. A. Ritchie, 1999: Effects of environmental flow upon tropical cyclone structure. *Mon. Wea. Rev.*, **127**, 2044, doi:10.1175/1520-0493(1999)127h2044: EOEFUTi2.0.CO;2.

Frank, W. M., and E. A. Ritchie, 2001: Effects of vertical wind shear on the intensity and structure of numerically simulated hurricanes. *Mon. Wea. Rev.*, **129**, 2249, doi: 10.1175/1520-0493(2001)129h2249:EOVWSOi2.0.CO;2.

George, J. E., and W. M. Gray, 1976: Tropical cyclone motion and surrounding parameter relationships. J. Appl. Meteor.,15, 1252–1264.

Goodyear, H. V., 1968: *Frequency and areal distributions of tropical storm rainfall in the United States coastal region on the Gulf of Mexico*, Vol. 7. US Department of Commerce, Environmental Science Services Administration, Weather Bureau.

Griffith, C. G., W. L. Woodley, P. G. Grube, D. W. Martin, J. Stout, and D. N. Sikdar, 1978: Rain estimation from geosynchronous satellite imagery visible and infrared studies. *Mon. Wea. Rev.*, **106**, 1153, doi:10.1175/1520-0493(1978)106h1153:REFGSIi2.0.CO;2.

Habib, E., A. Henschke, and R. F. Adler, 2009: Evaluation of TMPA satellite-based research and real-time rainfall estimates during six tropical-related heavy rainfall

events over Louisiana, USA. *Atmos. Res.*, **94**, 373–388, doi:10.1016/j.atmosres.2009.06.015.

Haggard, W. H., T. H. Bilton, and H. L. Crutcher, 1973: Maximum rainfall from tropical cyclone systems which cross the Appalachians. *J. Appl. Meteor.*, **12**, 50–61, doi:10. 1175/1520-0450(1973)012h0050:MRFTCSi2.0.CO;2.

Hence, D. A., and R. A. Houze, Jr., 2011: Vertical structure of hurricane eyewalls as seen by the TRMM precipitation radar. *J. Atmos. Sci.*, **68**, 1637–1652, doi: 10.1175/2011JAS3578.1.

HRD, cited 2017: Re-Analysis Project. [Available online at http://www.aoml.noaa.gov/hrd/hurdat/Data Storm.html].

Janjic, Z., T. Black, M. Pyle, H. Chuang, E. Rogers, and G. DiMego, 2005: The NCEP WRF NMM core. *Preprints, 2005 WRF/MM5 Users Workshop*, 27–30.

Jiang, H., J. B. Halverson, and J. Simpson, 2008: On the differences in storm rainfall from Hurricanes Isidore and Lili. Part I: Satellite observations and rain potential. *Wea. Forecasting*, **23**, 29, doi:10.1175/2007WAF2005096.1.

Jones, S. C., 1995: The evolution of vortices in vertical shear. i: Initially barotropic vortices. *Quart. J. Roy. Meteor. Soc.*, **121**, 821–851, doi:10.1002/qj.49712152406.

Kidder, S. Q., M. D. Goldberg, R. M. Zehr, M. Demaria, J. F. W. Purdom, C. S. Velden, N. C. Grody, and S. J. Kusselson, 2000: Satellite analysis of tropical cyclones using the advanced microwave sounding unit (AMSU). *Bull. Amer. Meteor. Soc.*, **81**, 1241–1260, doi:10.1175/1520-0477(2000)081h1241:SAOTCUi2.3.CO;2.

Kidder, S. Q., S. J. Kusselson, J. A. Knaff, R. R. Ferraro, R. J. Kuligowski, and M. Turk, 2005: The tropical rainfall potential (TRaP) technique. Part I: Description and examples. *Wea. Forecasting*, **20**, 456, doi:10.1175/WAF860.1.

Kurihara, Y., M. A. Bender, R. E. Tuleya, and R. J. Ross, 1995: Improvements in the GFDL hurricane prediction system. *Mon. Wea. Rev.*, **123**, 2791, doi:10.1175/1520-0493(1995) 123h2791:IITGHPi2.0.CO;2.

Lin, Y., and K. E. Mitchell, 2005: 1.2 the NCEP stage II/IV hourly precipitation analyses: Development and applications. *19th Conf. Hydrology, Amer. Meteor. Soc., San Diego, CA, USA*.

Lonfat, M., F. D. Marks, and S. S. Chen, 2004: Precipitation distribution in tropical cyclones using the tropical rainfall measuring mission (TRMM) microwave imager: A global perspective. *Mon. Wea. Rev.*, **132**, 1645, doi:10.1175/1520-0493(2004)132h1645: PDITCUi2.0.CO;2.

Lonfat, M., R. Rogers, T. Marchok, and F. D. Marks, 2007: A parametric model for predicting hurricane rainfall. *Mon. Wea. Rev.*, **135**, 3086, doi:10.1175/MWR3433.1.

Marchand, M., and H. Fuelberg, 2014: Assimilation of lightning data using a nudging method involving low-level warming. Mon. Wea. Rev., 142, 4850–4871, doi:https://doi.org/10.1175/MWR-D-14-00076.1.

Marchok, T., R. Rogers, and R. Tuleya, 2007: Validation schemes for tropical cyclone quantitative precipitation forecasts: Evaluation of operational models for u.s. landfalling cases. *Wea. Forecasting*, **22**, 726, doi:10.1175/WAF1024.1.

Marks, F., G. Kappler, and M. DeMaria, 2002: Development of a tropical cyclone rainfall climatology and persistence (R-CLIPER) model, paper presented at 25th conference on hurricanes and tropical meteorology. *Am. Meteorol. Soc., San Diego, Calif*.

Marks, F. D., Jr., R. A. Houze, Jr., and J. F. Gamache, 1992: Dual-aircraft investigation of the inner core of Hurricane Norbert. Part I: Kinematic structure. *J. Atmos. Sci.*, **49**, 919–942, doi:10.1175/1520-0469(1992)049h0919:DAIOTIi2.0.CO;2.

Pfost, R., 2000: Operational tropical cyclone quantitative precipitation forecasting. *Natl. Wea. Dig*, **24 (1-2)**, 61–66.

Reasor, P. D., R. Rogers, and S. Lorsolo, 2013: Environmental flow impacts on tropical cyclone structure diagnosed from airborne doppler radar composites. *Mon. Wea. Rev.*, **141**, 2949–2969, doi:10.1175/MWR-D-12-00334.1.

Riehl, H., and J. Malkus, 1961: Some aspects of Hurricane Daisy, 1958. *Tellus*, **13**, 181.

Roberts, and H. W. Lean, 2008: Scale-selective verification of rainfall accumulations from high-resolution forecasts of convective events. Mon. Wea. Rev., 136, 78–97, doi:10.1175/2007MWR2123.1.

Rogers, R., S. Chen, J. Tenerelli, and H. Willoughby, 2003: A numerical study of the impact of vertical shear on the distribution of rainfall in Hurricane Bonnie (1998). *Mon. Wea. Rev.*, **131**, 1577, doi:10.1175//2546.1.

Rogers, R., F. Marks, and T. Marchok, 2009: Tropical cyclone rainfall. *Encyclopedia of Hydrological Sciences*.

Schoner, R. W., 1968: *Climatological Regime of Rainfall Associated With Hurricanes After Landfall*. Weather Bureau, Eastern Region.

Schoner, R. W., and S. Molansky, 1956: *Rainfall Associated with Hurricanes (and Other Tropical Disturbances).* US Weather Bureau.

Scofield, R. A., and R. J. Kuligowski, 2003: Status and outlook of operational satellite precipitation algorithms for extreme-precipitation events. *Wea. Forecasting*, **18**, 1037, doi:10.1175/1520-0434(2003)018h1037:SAOOOSi2.0.CO;2.

Shapiro, L. J., 1983: The asymmetric boundary layer flow under a translating hurricane. *J. Atmos. Sci*, **40**, 1984–1998, doi:10.1175/1520-0469(1983)040h1984:TABLFUi2.0.CO;2.

Simpson, R. H., and H. Riehl, 1981: *The hurricane and its impact*. Louisiana State University Press.

Spayd, L. E., and R. A. Scofield, 1984: A tropical cyclone precipitation estimation technique using geostationary satellite data. Tech. rep., National Oceanic and Atmospheric Administration.

Villarini, G., and W. F. Krajewski, 2010: Review of the different sources of uncertainty in single polarization radar-based estimates of rainfall. *Surv. Geophys.*, **31**, 107–129, doi:10.1007/s10712-009-9079-x.

Villarini, G., J. A. Smith, M. L. Baeck, T. Marchok, and G. A. Vecchi, 2011: Characterization of rainfall distribution and flooding associated with U.S. landfalling tropical cyclones: Analyses of Hurricanes Frances, Ivan, and Jeanne (2004). *J. Geophys. Res.: Atmos.*, **116**, D23116.

Wilks, D. S., 2006: *Statistical methods in the atmospheric sciences*, Vol. 91. Second edition ed., Academic press.

Wingo, M. T., and D. J. Cecil, 2010: Effects of vertical wind shear on tropical cyclone precipitation. *Mon. Wea. Rev.*, **138**, 645–662, doi:10.1175/2009MWR2921.1.

Xu, W., H. Jiang, and X. Kang, 2014: Rainfall asymmetries of tropical cyclones prior to, during, and after making landfall in South China and Southeast United States. *Atmos. Res.*, **139**, 18–26, doi:10.1016/j.atmosres.2013.12.015.

Yang, F., Cited 2017: GFS Performance Review 2015. [Available online at https://vlab.ncep.noaa.gov/web/gfs/home/-/document_library_display/m9Q6Ukcv8EV2/view/849649].

Zagrodnik, J. P., and H. Jiang, 2013: Investigation of PR and TMI Version 6 and Version 7 rainfall algorithms in landfalling tropical cyclones relative to the NEXRAD Stage-IV multisensor precipitation estimate dataset. *J. Appl. Meteor. Climatol.*, **52**, 2809–2827, doi:10.1175/JAMC-D-12-0274.1.